The failure behavior of prefabricated fractured sandstone with different rock bridge inclination angles under freeze-thaw cycles

Meilu Yu [a], Zhongwen Wang [a,*], Ying Xu [a,b], Yanhai Chang [a], Luyu Wang [c], Yulong Zhu [d]

[a] State Key Laboratory of Mining Response and Disaster Prevention and Control in Deep Coal Mines, Anhui University of Science and Technology, Anhui, China
[b] School of Civil Engineer and Architecture, Anhui University of Science and Technology, Huainan, China
[c] Department of Civil and Environmental Engineering, The Hong Kong Polytechnic University, Hong Kong, China
[d] School of Environment and Energy Engineering, Anhui Jianzhu University, Hefei, China

ABSTRACT

In this paper, the fractured rock samples with different dip angles of rock bridge are taken as the research object, and the freeze-thaw cycle test and uniaxial compression test are carried out successively. Combined with digital image correlation technology (DIC) and numerical simulation, the failure process of prefabricated fractured sandstone with different rock bridge dip angles was studied. The results show that the frost heaving force caused by freezing and thawing will cause irreversible damage to the rock sample. Especially at the tip of the pre-fabricated crack, macroscopic frost heaving cracks will occur. Frost heaving cracks can reduce the stress concentration at the crack tip, which leads to a decrease in tensile cracks during loading. With the increase of the inclination angle of the rock bridge, both the modulus and the peak stress show an inverted "spoon-shaped" trend of increasing first and then decreasing. The tensile effect of the frost heave force generated by the freeze-thaw process leads to the early development and expansion of the prefabricated cracks. Under the action of external load, according to the law of crack development, the failure mode of rock bridge can be divided into shear failure (S type), tensile failure (T type) and tensile-shear composite failure (M type). The relative displacement evolution curve of the characteristic points on both sides of the fracture surface is basically consistent with the evolution characteristics of the strain field. According to whether the *x*-direction and *y*-direction displacement curves of the feature points deviate from each other, the type of driving force of fracture propagation can be judged.

1. Introduction

Rock mass instability caused by freeze-thaw damage is a common natural disaster in alpine regions [1,2]. The rock slope of Yulong Copper Mine in Xizang is often broken due to the influence of freeze-thaw action and excavation stress. Its stability evaluation and disaster prevention become urgent [3,4]. The initial damage structures such as pores, joints, cracks and discontinuous planes formed in the rock under the long geological and environmental effects cause the heterogeneity of the rock [5]. The inhomogeneity of rock has an important influence on its failure process, failure mode and macroscopic mechanical properties [6–8]. Especially in the low temperature environment, the freezing and thawing alternate day and night in the cold region, and the microscopic

damage inside the rock accelerates [9,10]. The rock bridge is defined as a complete region between two adjacent discontinuous joint tips. Under the action of external load, the mineral particles slip and dislocate, which promotes the continuous initiation and expansion of microcracks in the rock. The initial damage areas of the rock are connected to each other, resulting in the connection of the rock bridge area. The intermittent structural plane quickly develops into a connected slip surface, which eventually leads to the loss of bearing capacity of the rock and causes a series of engineering disasters [11–13]. The continuous freezing-thawing process leads to the gradual increase of fracture aperture, which causes the deterioration of rock micro-damage, frost heave fragmentation and failure instability, and then becomes the potential cause of geological disasters such as rockfall and landslide in cold

regions [12,14–16]. The pre-existing defects in the rock mass dominate the deformation and failure process, including the initiation, propagation and merging of new cracks generated by the pre-existing defect tips. Therefore, it is of great significance for rock engineering in cold regions such as rock slopes, rock foundations and tunnels to understand the mechanical properties and cracking process of defective rocks under freeze-thaw cycles and loads.

In recent years, scholars have done a lot of research on the mechanical properties of fractured rocks in cold regions under freeze-thaw action from different angles [17–20]. Based on the rock occurrence environment in cold region, the stress-strain curves of rock under freeze-thaw and confining pressure conditions are studied, and the relationship between rock mechanical parameters and confining pressure under freeze-thaw conditions is analyzed [21,22]. Based on the geometric parameters of cracks, the effects of freeze-thaw cycles, geometric parameters of cracks and confining pressure on mechanical properties were studied, and the failure modes of rock samples were summarized [23–25]. With the increase of rock engineering problems in cold regions, scholars have found that the instability and failure of rock engineering are closely related to crack propagation, and confirmed that in almost all rock engineering projects, the structures in or on the rock mass contain both cracks and rock bridges [26–29]. The existence of cracks and rock bridges is not only an important factor affecting the mechanical response of rock mass, but also the interaction between the two and the failure of rock bridges control the mechanical behavior of fractured rock mass and the stability of rock excavation [30,31]. The cracks and joints inside the rock mass interact with the stress field, resulting in new cracks [32,33]. With the continuous expansion of cracks, they begin to interact, overlap and penetrate with other cracks, making them unstable until the newly separated plane is destroyed. The destruction of the rock bridge causes the macroscopic failure of the rock mass, which ultimately threatens the stability and safety of the project construction [34,35]. From the above research, it can be seen that great progress has been made in the study of mechanical properties and failure modes of fractured rock. Crack coalescence in rock bridges is usually the cause of many rock structure failures. The macroscopic instability failure mode of fractured rock in cold region is a complex process. It is difficult to summarize the failure mechanism of fractured rock in cold region only considering the mechanical properties and failure mode. With the application of digital image correlation technology in the field of rock mechanics, it can well monitor and record the failure process of fractured rock. Many scholars have carried out a lot of work from the aspects of crack initiation, propagation and evolution. Sharafisafa et al. [36] studied the mechanism of crack initiation, propagation and coalescence by using single and double defect specimens, and determined that tensile coalescence was the main behavior of double defect specimens under load, while shear coalescence was difficult to occur. Zhou et al. [37] studied the crack development mechanism of brittle and ductile specimens with multiple pre-existing defects under uniaxial compression tests. Shirole et al. [38] studied the heterogeneity of multi-scale strain field in rocks by DIC method. analyzed the progressive failure mechanism of rock tunnels with fault zones. Therefore, it is of great theoretical value and engineering significance to monitor and record the crack propagation law caused by the existence and arrangement of rock bridges with the help of digital image correlation technology to explore the failure behavior of fractured rock in cold regions.

In engineering, the environment is diverse, the geometry is diverse, and the mechanical environment is complex and changeable. Numerical simulation has the characteristics of low cost, fast speed, and repeatability, making numerical simulation an indispensable analytical method for solving scientific problems. The failure process of rock is a process from micro-crack initiation to local failure and then to macroscopic failure. During the loading process, the stress state and displacement mode of rock particles determine the crack type and propagation direction. The Discrete Element Method (DEM), which does

not require complex constitutive relations, has advantages in characterizing the microstructure of rock. It is helpful to understand the crack propagation law and the micro evolution mechanism of crack. Ju et al. [39] The crack propagation behavior and its effect on the macro-crack resistance of jointed rock were evaluated by discrete element modeling (DEM). Zare et al. [40] studied the effects of contact area and number of rock bridges, normal load, angle, length and number of joints on the shear strength of non-persistent rock joints. Xu et al. [41] The effects of fracture length and fracture dip angle on rock cracking behavior were investigated by experiments and numerical simulations, and four failure modes were obtained in the rock bridge area. Wu and Huang [42] discussed the stress distribution at the crack tip and the local stress evolution around the crack based on two kinds of crack evolution behaviors.

In summary, it is found that most of the research results are based on single and double prefabricated cracks. The influence mechanism of crack length and dip angle on the mechanical properties and failure characteristics of fractured rock mass under load is deeply analyzed, but it is neglected that rock bridge is the main factor controlling the mechanical behavior of fractured rock mass and the stability of rock excavation. Therefore, it is necessary to study the fractured rock with different dip angles of rock bridge, explore the change law of its mechanical properties, and reveal the failure and instability mechanism of rock bridge area. In view of this, this paper takes fractured rock samples with different rock bridge dip angles as the research object, and has carried out freeze-thaw cycle test and uniaxial compression test successively. The failure process of fractured rock was studied by digital image correlation (DIC). Finally, the freeze-thaw model of fractured rock is constructed by DEM, and the influence mechanism of freeze-thaw cycle on the deformation of fracture surface is discussed, and the bearing capacity of fractured rock with different rock bridge dip angles is evaluated. The research results can provide a theoretical basis for the prevention and control of rock slope disasters in Yulong Open-pit Mine in Tibet.

2. Test scheme

2.1. Engineering background

This study takes the Yulong Copper Mine in Jiangda County, Changdu City, Xizang Autonomous Region, China as the research object, as shown in Fig. 1b. The altitude of the mining area is 4569–5118 m, the average daily minimum temperature of the coldest month is −20 °C, and the freezing period in one year is more than 7 months. The stability of the mine rock slope is significantly affected by freeze-thaw cycle [43, 44]. The instability mode of stepped failure often occurs in rock slopes with joints and cracks, and its stability is mainly controlled by structural planes and rock bridges. Because the rock bridge is the shortest path of all potential sliding surfaces, the sliding surface is usually formed between the cracks. In the process of open-pit slope excavation, the original stress equilibrium state is broken, and a large stress concentration occurs at the joint tip, which leads to the initiation, propagation and penetration of cracks around the rock bridge. Finally, the rock loses its bearing capacity and causes a series of engineering disasters. Therefore, it is of great theoretical guiding significance, academic value and social benefits for the safe and efficient exploitation of mineral resources in cold regions to explore the evolution characteristics of joint crack initiation, expansion and penetration.

The rock from Yulong mining area is prepared as a cube with length, width and height of 50 * 50 * 100 mm. In this experiment, non-overlapping penetrating cracks are used, and the specific distribution form is shown in Fig. 1d (e). The length of the fissure is $2c$, the width of the fissure is a, the dip angle of the fissure is α, the dip angle of the rock bridge is β, and the length of the rock bridge (the distance between the tip II in the two prefabricated fissures) is $2b$. In order to simplify the study, $2c = 20$ mm, $2b = 10$ mm, $\alpha = 45°$, $a = 2$ mm and $\beta = 30°, 45°$,
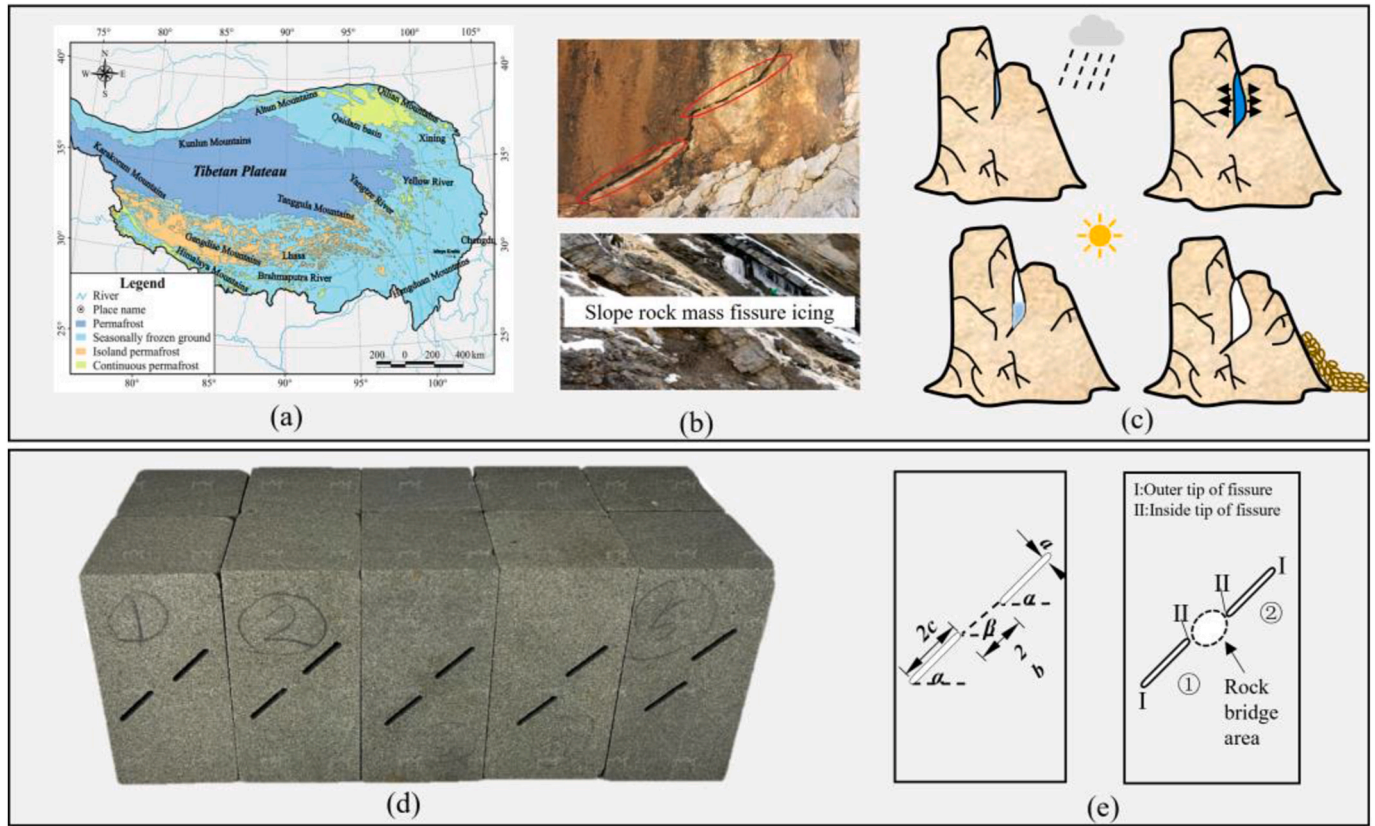
Fig. 1. Preparation of fractured rock samples with different dip angles of rock bridge.
(a) Distribution of permafrost in Qinghai-Tibet Plateau [45] (b) Fractured rock mass affected by freeze-thaw (c) Potential hazards of rock mass caused by freezing and thawing, (d) Preparation of fractured rock mass, (e) Geometric distribution characteristics of cracks.

60°, 75°, 90°.

2.2. Experimental equipment and process

Reference ISRM specification and freeze-thaw cycle operating standards, and based on the actual working conditions of the day and night temperature difference in the mining area, as well as other scholars experience in setting parameters for freeze-thaw cycle tests [46]. The freeze-thaw cycle test parameters are set as follows: the freezing temperature is $-20\,°C$, the dissolution temperature is $20\,°C$, and the first freeze-thaw cycle is 10 h, in which the freeze-thaw time is 5 h, the melting time is 5 h, and the freezing and melting speed are both $8\,°C/h$. The samples with different rock bridge dip angles were subjected to 80 freeze-thaw cycle tests. Uniaxial compression test loading equipment using RMT rock mechanics testing machine. The uniaxial compression test was carried out on the fractured rock samples after freeze-thaw cycles, and the displacement loading control was adopted at a rate of 0.02 mm/min.

The specific test process.

(1) After removing the samples with uneven surface and large discreteness, a total of 10 rock samples were selected, as shown in Fig. 2a. The rock samples are divided into 5 groups according to the different dip angles of the rock bridge, and each group has two samples. As shown in Table 1.

As shown in Table 1, the sample number is R-30-1, R is expressed as a rock sample, 30 is expressed as a rock bridge dip angle β, and 1 is expressed as the first sample in each group.

(2) The screened rock samples are placed in an oven and dried at 110° for 48 h to constant weight, as shown in Fig. 2b;

(3) The dry rock sample was put into distilled water and saturated for 48 h by vacuum pumping method, as shown in Fig. 2c;

(4) The surface of the saturated rock sample is wiped clean and wrapped with a preservative film, so that there is no water on the surface of the rock sample and in the prefabricated cracks, as shown in Fig. 2d;

(5) Put the rock samples into the high and low temperature (alternating) test chamber in turn, carry out 80 freeze-thaw cycles, and the temperature evolution curve is shown in Fig. 3. Freeze-thaw damage rock samples, as shown in Fig. 4;

(6) The static compression test of freeze-thaw damage rock samples was carried out by using RMT-150C rock mechanics test system. The axial deformation of rock can be measured by a displacement sensor with a range of 5 mm and a stroke sensor with a range of 50 mm in the rock mechanics test system. At the same time, DIC technology was used to monitor the evolution characteristics of the surface deformation field of the sample, as shown in Fig. 2 (f).

From Fig. 4 that when the dip angle of the rock bridge is $\beta \leq 45°$, only far-field cracks appear on the surface of the specimen. When the dip angle of the rock bridge is $\beta > 45°$, the frost heave crack first starts from the crack tip, expands along the coplanar direction of the crack, and then extends to the side and back of the sample to form a penetrating frost heave crack. This results in different degrees of damage to rock samples with different rock bridge dip angles before uniaxial compression test.

Under the action of F-T cycle, the surface of the sample is more likely to be damaged (Fig. 4), and the rock samples with different rock bridge dip angles have different degrees of damage, which is basically consistent with the study of Zhu et al. [47]. With the increase of the inclination
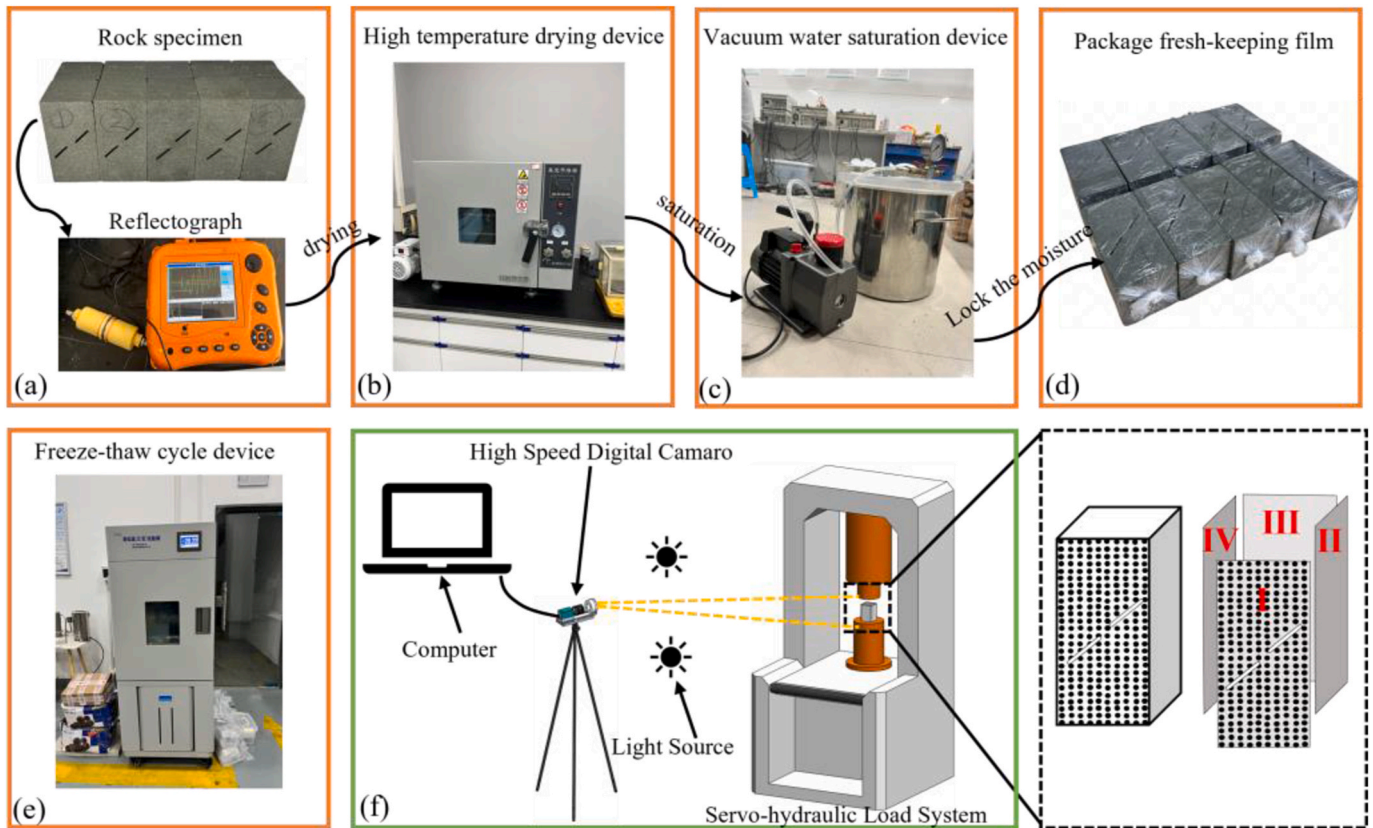
Fig. 2. Different rock bridge sample test process.

Table 1
Sample grouping.

Sample number	rock bridge dip angle/°	rock bridge length/ mm	fracture dip angle/°	fracture width/ mm	fissure length/ mm	freeze-thaw cycles
R-30-1	30	10	45	2	20	80
R-30-2	30	10	45	2	20	80
R-45-1	45	10	45	2	20	80
R-45-2	45	10	45	2	20	80
R-60-1	60	10	45	2	20	80
R-60-2	60	10	45	2	20	80
R-75-1	75	10	45	2	20	80
R-75-2	75	10	45	2	20	80
R-90-1	90	10	45	2	20	80
R-90-2	90	10	45	2	20	80

Fig. 3. Temperature evolution curve.

angle of the rock bridge, the damage of the sample surface is more obvious, especially in the rock bridge area. When the dip angle of the rock bridge is small ($\beta \leq 45°$), a small number of cracks appear on the surface of the sample and are far away from the rock bridge area. When the dip angle of the rock bridge is large ($\beta > 45°$), the frost heave cracks first crack from the crack tip and propagate along the coplanar direction of the crack (Fig. 4c, d, and e). These freeze-thaw damage is mainly based on the weathering and spalling of the surface, with some micro cracks on the surface. Because the freezing effect starts from the surface of the rock sample, the surface of the rock sample is damaged first. The surface damage is greater than the internal damage.
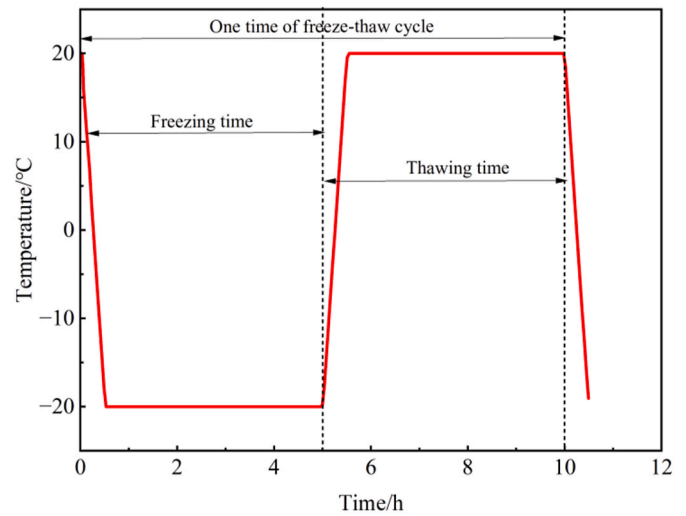
3. Test result analysis

3.1. Stress-strain curve

The stress-strain curves of fractured rock samples under different dip angles of rock bridge are shown in Fig. 5. Through the analysis of the stress-strain curve, it is found that the stress-stress curve of the fractured rock sample shows a similar trend under different rock bridge dip angles. At the initial stage of loading, the original open structural plane or micro-fissure in the rock gradually closed, and the rock was in the compaction stage. Elastic deformation stage: the stress-strain curve is
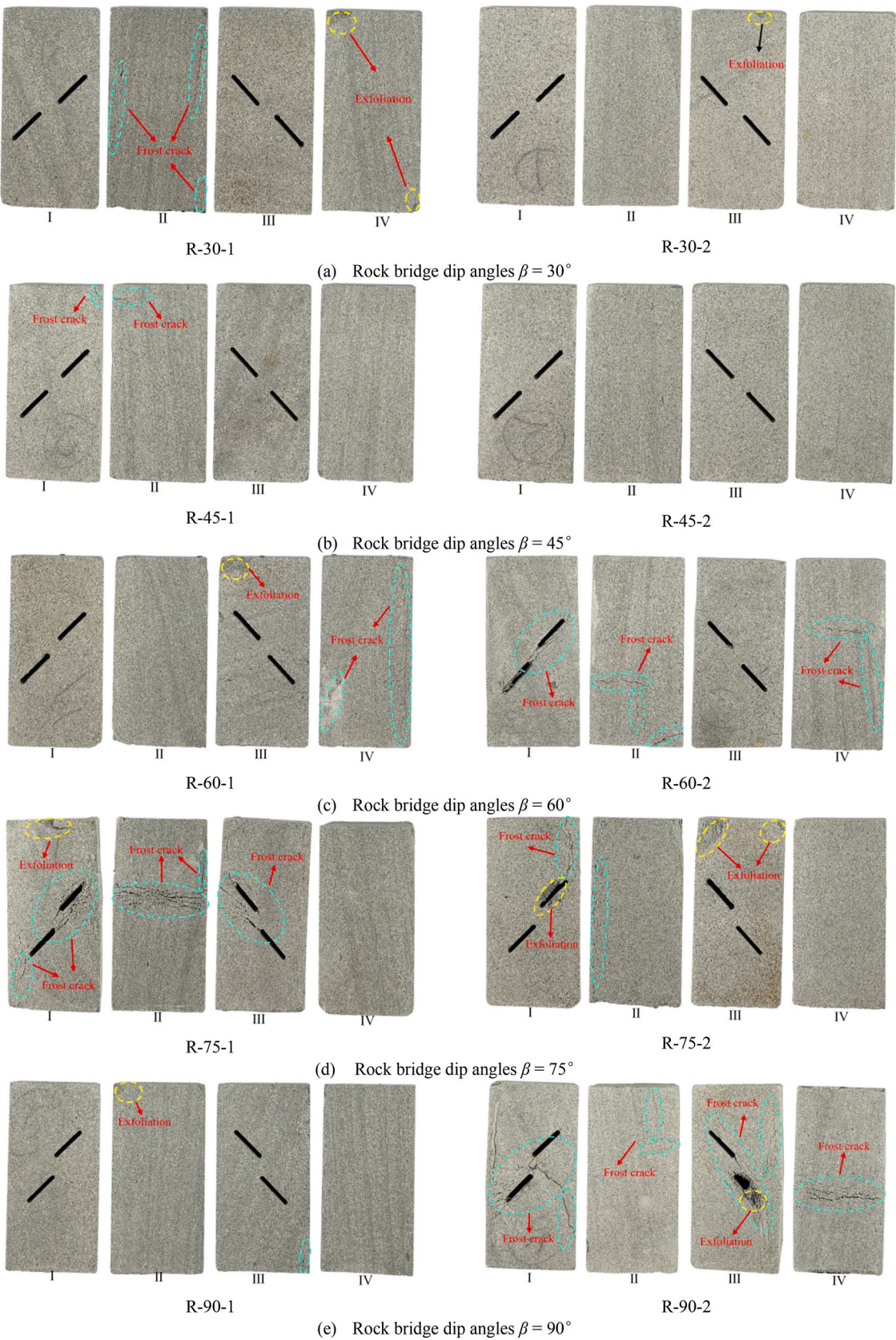
(a) Rock bridge dip angles $\beta = 30°$

(b) Rock bridge dip angles $\beta = 45°$

(c) Rock bridge dip angles $\beta = 60°$

(d) Rock bridge dip angles $\beta = 75°$

(e) Rock bridge dip angles $\beta = 90°$

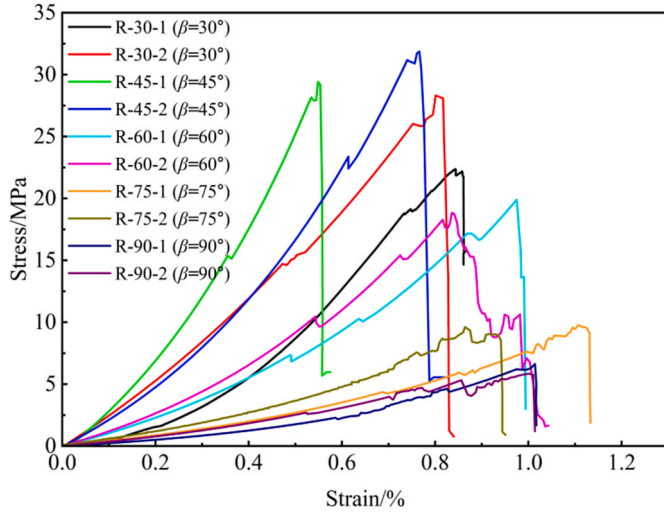**Fig. 4.** Samples with different dip angles of rock bridge under the same number of freeze-thaw cycles.

Fig. 5. Stress-strain curves of specimens with different rock bridge dip angles.

approximately linear. The stable development stage of crack: the slope of the stress-strain curve decreases with the increase of stress, and the microcracks begin to initiate, but the microcracks are controlled by the applied load. The unstable propagation stage of cracks: the stress-strain curve is convex, and the cracks continue to develop until the sample is completely destroyed.

From Fig. 5 that the rock samples with different rock bridge dip angles have different degrees of nonlinear deformation in the initial stage of loading, which is mainly caused by the gradual closure of the initial pores or cracks of the rock samples. Since then, the elastic deformation began to dominate the stress-strain curve, and the stress and strain were approximately linear. However, when cracks begin to initiate near the tip of the prefabricated crack or the rock bridge area, a significant stress drop can be observed on the curve. After several times of stress drop, the specimen will quickly reach the peak strength, and unstable failure will occur with the increase of axial deformation.

3.2. Effect of dip angle of rock bridge on deformation and strength parameters

The initial modulus reflects the number of micro cracks in the rock, the secant modulus reflects the overall deformation characteristics of the rock, and the elastic modulus reflects the ability of the rock to resist elastic deformation and the degree of deformation. As shown in Fig. 6.

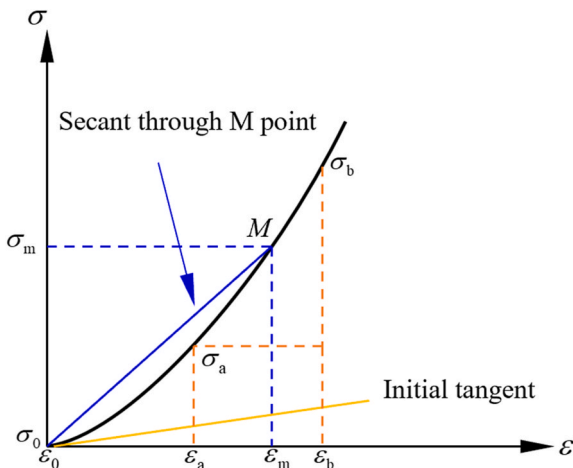The initial modulus: the slope of the stress-strain curve at the origin

tangent, as shown in Eq. (1):

$$E_0 = \frac{d\sigma_0}{d\varepsilon_0}\bigg|_{\varepsilon=0} \tag{1}$$

where E_0 is the initial modulus of the specimen, GPa; σ_0 is the stress at the origin of the stress-strain curve, MPa; ε_0 is the strain value at the origin of the stress-strain curve.

The secant modulus: The slope of the secant at point M corresponding to 50 % of the ultimate strength in the stress-strain curve, shown in Eq. (2):

$$E_s = \frac{\sigma_m - \sigma_0}{\varepsilon_m - \varepsilon_0} \tag{2}$$

where E_s is the secant modulus of the sample, GPa; σ_m is the stress value of M point, MPa; ε_m is the axial strain value corresponding to σ_m.

Elastic modulus: the slope of the line connecting the starting point of the elastic line stage to the end point of the elastic line stage in the stress-strain curve, as shown in Eq. (3):

$$E_e = \frac{\sigma_b - \sigma_a}{\varepsilon_b - \varepsilon_a} \tag{3}$$

Where E_e is the elastic modulus of the sample, GPa; σ_a is the stress value at the starting point of the elastic line segment, MPa; σ_b is the stress value at the end of the elastic segment, MPa; ε_a and ε_b are the corresponding axial strain values when the axial stress is σ_a and σ_b respectively.

Through Eqs. (1) and (3), the initial modulus, secant modulus and elastic modulus and peak strength, as shown in Table 2. The average value of the modulus and the average value of the peak strength change with the inclination of the rock bridge, as shown in Fig. 7.

From Fig. 7a, it can be seen that the evolution of the three with the change of the dip angle of the rock bridge shows an inverted "spoon-shaped" evolution law of rising first and then falling. When $\beta > 45°$, the three modulus values decrease with the increase of the dip angle of the rock bridge. When $\beta \leq 45°$, the three modulus values increase with the increase of dip angle of rock bridge. When $\beta = 45°$, the three modulus values are the largest. When the dip angle of rock bridge is the same, the size of three kinds of modulus is shown as elastic modulus > secant modulus > initial modulus. From Fig. 7b that the peak stress also exhibits the same evolution law as the modulus.

3.3. The influence of rock bridge dip angle on the evolution law of rock failure

Rock is a non-homogeneous material. When the load is large, stress concentration will occur in the local area. When the load exceeds the maximum compressive strength of the rock, new cracks (such as wing crack, coplanar crack, quasi-coplanar crack and secondary inclined crack) will be initiated here, and expand with the increase of load until the sample is unstable and destroyed [48]. In order to deeply analyze the law of crack development, one rock sample from each group was selected for analysis, as shown in Figs. 8–12.

Fig. 8 shows the cracking process of R-30-2 ($\beta = 30°$) specimen. From Fig. 8, it can be seen that when the loading is up to 157 s, the wing crack T-1 and T-2 begin to initiate from the outer tip I of fissure ① and ②, respectively, and expand along the loading direction. When loaded to 173 s, the wing crack T-3 initiates from the inside tip II of fissure ①. When loaded to 215 s, the wing crack T-4 starts to initiate from the inside tip II of fissure ②. The propagation directions of T-3 and T-4 wing cracks are perpendicular to the prefabricated fissure. At this time, the wing cracks T-1 and T-2 have penetrated the sample, and the rock bridge area is penetrated by the secondary inclined crack S-1. The final specimen failed, and the wing crack T-5 and the secondary inclined crack S-1 lapped, and the spalling phenomenon occurred in the rock bridge area.

Fig. 9 shows the cracking process of the specimen numbered R-45-2

Fig. 6. Deformation characteristics of rock.

Table 2
Strength and modulus of specimens under different rock bridge dip angles.

Sample number	Rock bridge dip angles/°	Initial modulus/GPa		Secant modulus/GPa		Elastic modulus/GPa		Peak stress/GPa	
		Test value	Mean value	Test value	Mean value	Test value	Mean value	Test value	Mean value
R-30-1	30	2.81	2.77	3.49	3.33	4.41	4.19	28.30	25.32
R-30-2		2.72		3.16		3.96		22.33	
R-45-1	45	3.74	3.55	4.84	4.49	5.99	6.12	29.40	30.63
R-45-2		3.35		4.13		6.25		31.86	
R-60-1	60	1.39	1.35	1.89	2.11	2.94	2.91	19.91	19.36
R-60-2		1.30		2.32		2.87		18.80	
R-75-1	75	0.47	0.51	0.79	0.84	1.22	1.25	9.74	9.68
R-75-2		0.54		0.88		1.27		9.62	
R-90-1	90	0.29	0.36	0.52	0.55	0.62	0.66	6.42	6.13
R-90-2		0.42		0.58		0.69		5.84	

(a) Three kinds of modulus

(b) Peak stress

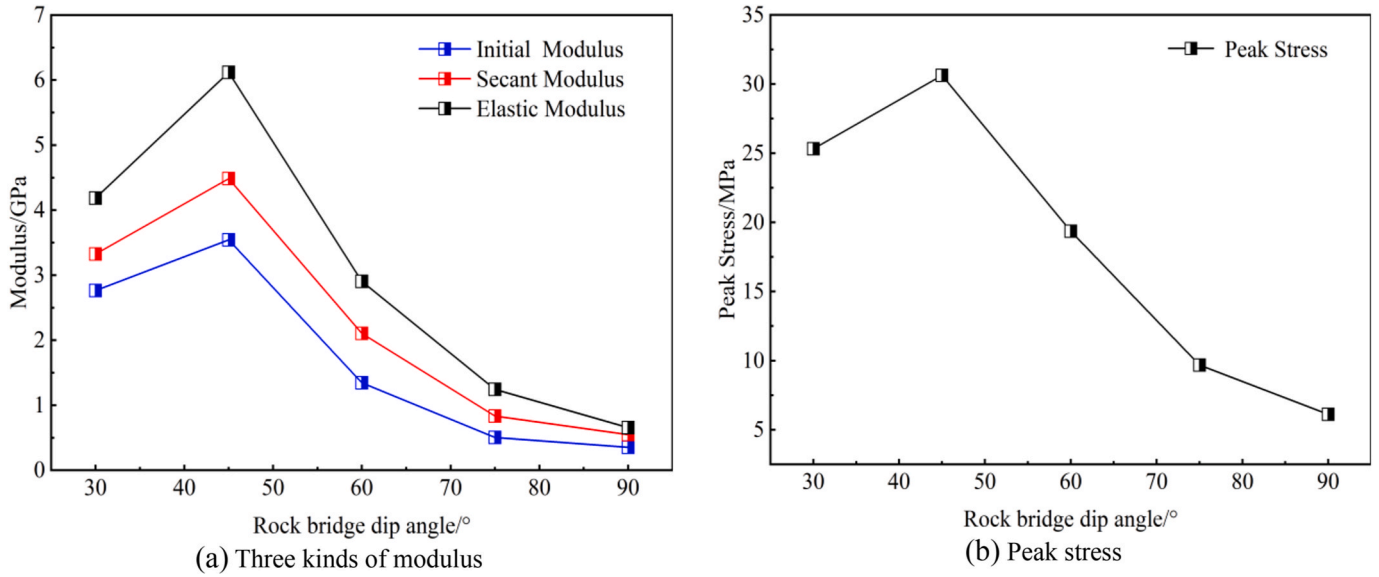**Fig. 7.** Relationship between deformation parameters and dip angle of rock bridge.

I - outer tip of fissure; II-Inside tip of fissure; ① - Prefabricated fissure below; ② - Prefabricated fissure above
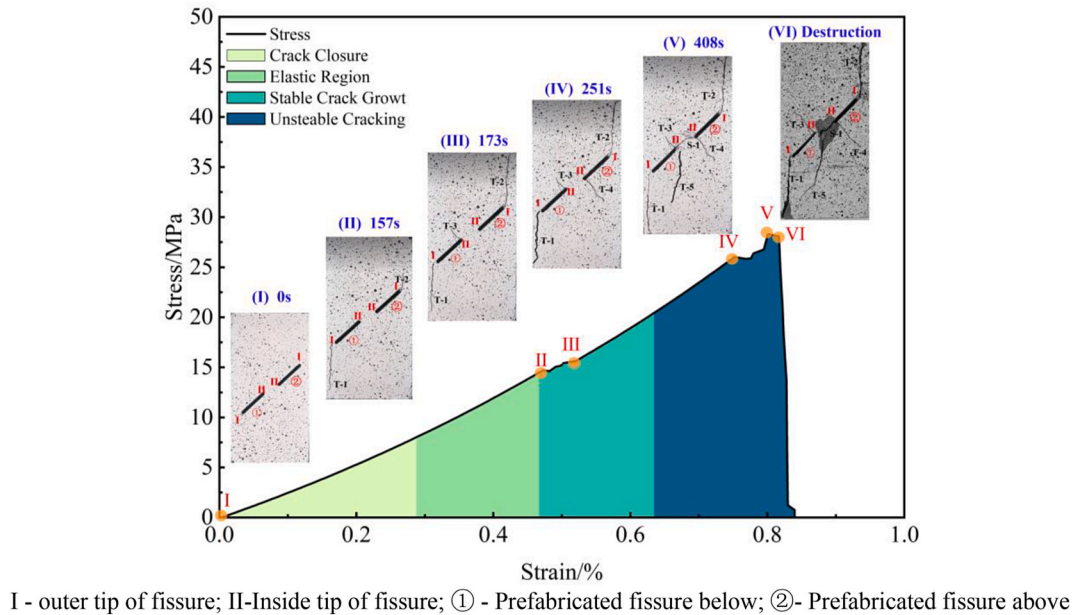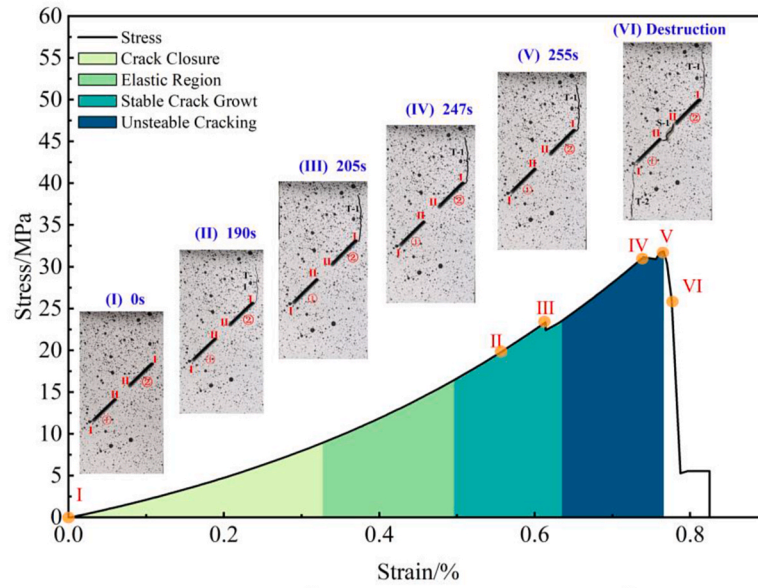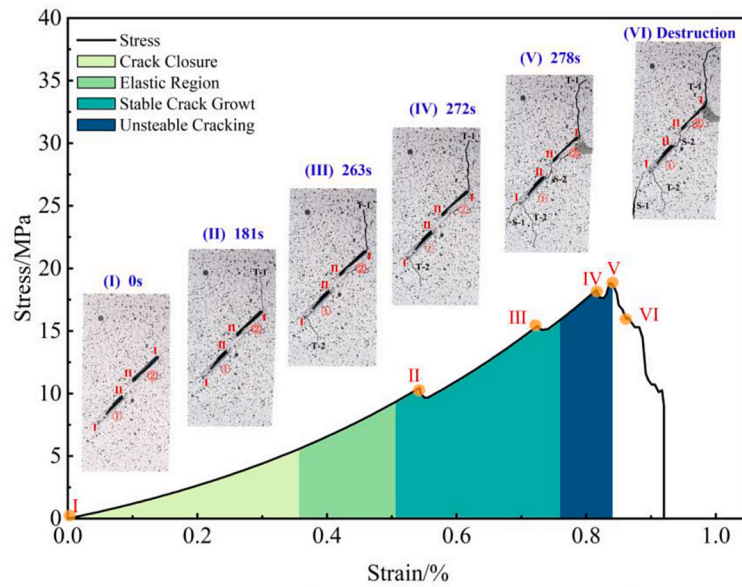
Fig. 8. Cracking process of rock bridge dip angle $\beta = 30°$ specimen.

I - outer tip of fissure; II-Inside tip of fissure; ① - Prefabricated fissure below; ②- Prefabricated fissure above

Fig. 9. Cracking process of rock bridge dip angle $\beta = 45°$ specimen.

I - outer tip of fissure; II-Inside tip of fissure; ① - Prefabricated fissure below; ②- Prefabricated fissure above

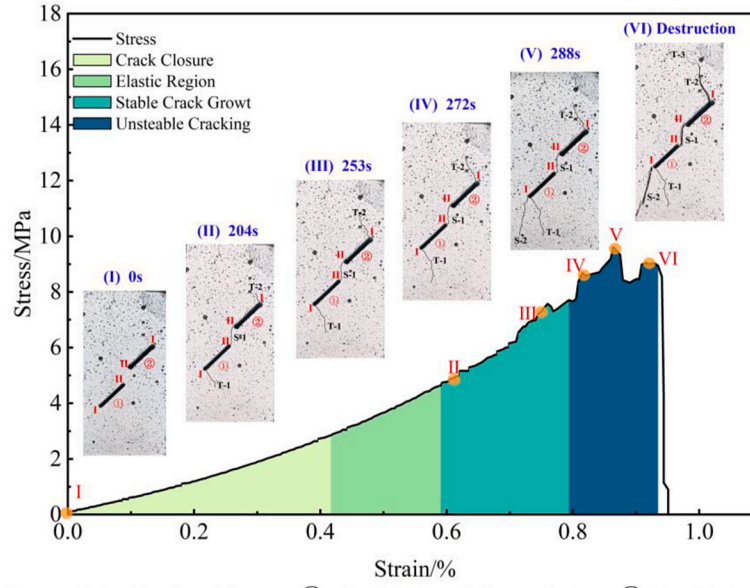**Fig. 10.** Cracking process of rock bridge dip angle $\beta = 60°$ specimen.

($\beta = 45°$). From Fig. 9, it can be seen that when the loading is up to 190 s, the wing crack T-1 starts from the outer tip I of fissure ② and expands along the loading direction. Until 255 s, the wing crack T-1 extends through the sample, and no other cracks appear. With the continuous increase of axial stress, the secondary crack S-1 and the wing crack T-2 appear almost at the same time, which penetrate the rock bridge area and the specimen respectively, causing the instability failure of the specimen.

Fig. 10 shows the cracking process of the specimen numbered R-60-2 ($\beta = 60°$). It can be seen from Fig. 10 that when loaded to 181 s, the wing crack T-1 first initiates from the outer tip I of fissure ① and propagates along the loading direction. When loading to 263 s, the wing crack T-2 starts to initiate from the outer tip I of the fissure ①, and its propagation direction is perpendicular to the prefabricated crack. When loaded to 278 s, quasi-coplanar crack S-1 and coplanar crack S-2 appear almost

simultaneously. Finally, the quasi-coplanar crack S-1 penetrates the specimen, and the coplanar crack S-2 directly penetrates the rock bridge area.

Fig. 11 is the cracking process of the specimen numbered R-75-2 ($\beta = 75°$). It can be seen from Fig. 11 that when loaded to 204 s, wing cracks T-1, T-2 and secondary inclined cracks S-1 almost appear on the surface of the sample. Wing crack T-1 and wing crack T-2 initiate from the outer tip I of fissure ① and fissure ② respectively, and their propagation directions are perpendicular to the prefabricated crack. The secondary inclined crack S-1 is extended from the inside tip II of fissure ① to the inside tip II of fissure ② along the direction of the rock bridge, so that the rock bridge area is penetrated. When loaded to 288 s, the secondary inclined crack S-2 initiates from the outer tip I of fissure ①, and rapidly expands and penetrates the specimen. At the moment of specimen failure, the propagation direction of wing crack T-2 is deflected, forming

I - outer tip of fissure; II-Inside tip of fissure; ① - Prefabricated fissure below; ②- Prefabricated fissure above

Fig. 11. Cracking process of rock bridge dip angle $\beta = 75°$ specimen.
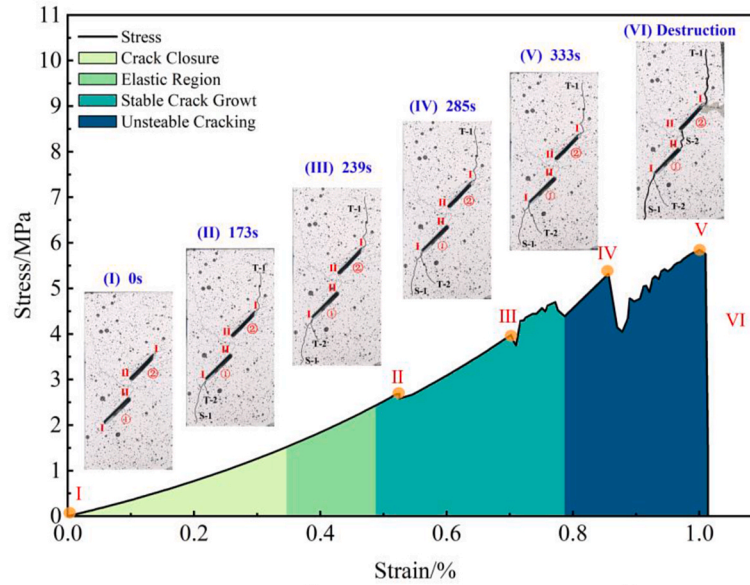
I - outer tip of fissure; II-Inside tip of fissure; ① - Prefabricated fissure below; ②- Prefabricated fissure above

Fig. 12. Cracking process of rock bridge dip angle $\beta = 90°$ specimen.

wing crack T-3.

Fig. 12 shows the cracking process of the specimen numbered R-90-2 ($\beta = 90°$). It can be seen from Fig. 12 that when loaded to 173 s, wing cracks T-1, T-2 and secondary inclined cracks S-1 almost appear on the surface of the sample. The wing crack T-1 initiates from the outer tip I of fissure ② and propagates along the loading direction. Although both wing crack T-2 and secondary inclined crack S-1 start from the outer tip I of fissure ①, their propagation directions are very different. The propagation direction of wing crack T-2 is perpendicular to the prefabricated crack, while the secondary inclined crack S-1 propagates along the loading direction. Before the instability failure of the sample, no other cracks appeared, while T-1, T-2 and S-1 continued to develop and expand, and finally the secondary crack S-2 penetrated the rock bridge area.

In summary, it can be seen that the wing cracks initiated at the tip of

the prefabricated crack cause the tensile penetration of the sample and the secondary crack penetration of the rock bridge area, which eventually causes the overall failure of the rock sample. The tension penetration of the specimen is caused by the wing crack, which causes the stress concentration in the rock bridge area, but the specimen still has the bearing capacity at this time. The rock bridge is the shortest path of all potential sliding surfaces. When the rock bridge area is penetrated, the specimen will fail.

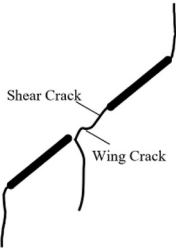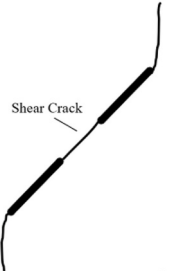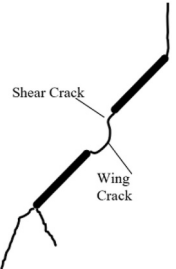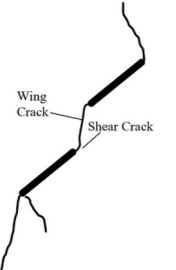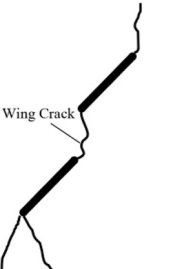### 3.4. The failure mode of rock bridge penetration

Through the analysis of the above rock failure evolution law, it can be seen that the rock bridge penetration is the main reason for the rock instability failure. The rock bridge penetration is closely related to the development of the prefabricated crack tip. In order to deeply analyze

the failure mechanism of fractured rock. This section summarizes the failure characteristics of the rock bridge through the rock sample, as shown in Table 3. The shear crack slides along the crack direction, and the propagation direction is parallel to the prefabricated crack. The wing crack initiation direction forms a certain angle with the crack surface. From Table 3, two main types of cracks can be identified in the rock bridge area of the sample: Wing crack (tensile crack), secondary crack (shear crack). Based on the two types of cracks and their combinations,

three types of rock bridge penetration modes (S-type, T-type, M-type) are summarized, as shown in Fig. 13.

When the shear cracks in the rock bridge area play a leading role and connect with each other through the whole rock bridge, it can be judged as S-type failure mode. When the tensile crack in the rock bridge area plays a leading role and expands through the rock bridge in the rock bridge ar-ea, it can be judged as a T-type failure mode. When there are wing cracks (tensile cracks) and secondary cracks (shear) in the rock

Table 3
Failure charanteristics and mechanism of rock samples.

| Sample number	Rock bridge dip angles/°	Crack propagation morphology	Characteristics of rock bridge penetration	failure characteristics
R-30-2	30°		Secondary shear cracks appear in the overlap of wing cracks, which penetrate the whole rock bridge area.	Less pull-more shear mixed failure
R-45-2	45°		High shear stress promotes the propagation of secondary shear cracks through the whole rock bridge area.	Direct shear failure
R-60-2	60°		The wing crack extends to part of the rock bridge and is connected with the secondary shear crack, which penetrates the whole rock bridge area.	More pull less shear mixed failure
R-75-2	75°		The wing crack extends to part of the rock bridge and is connected with the secondary shear crack, which penetrates the whole rock bridge area.	More pull less shear mixed failure
R-90-2	90°		During loading, the tensile stress causes the two wing cracks to merge and penetrate the rock bridge area.	Indirect tensile failure
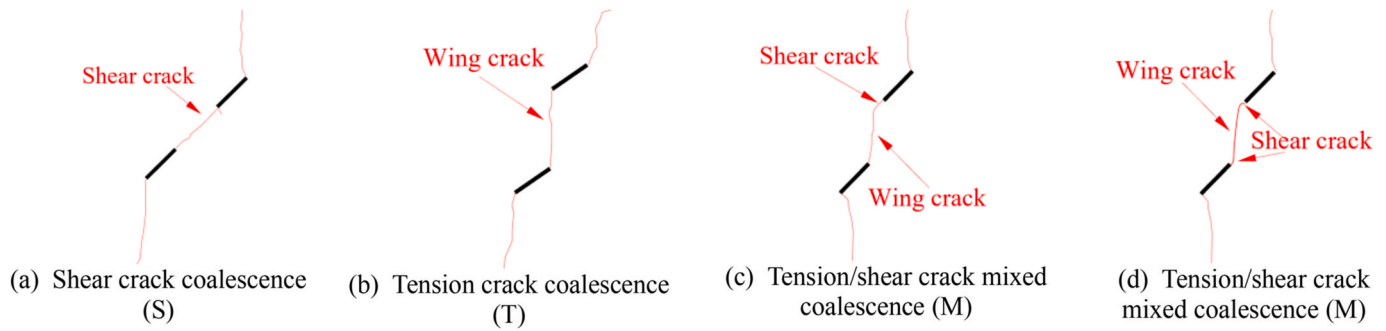
Fig. 13. Five different patterns of crack coalescence observed in our experiments.

bridge area, and the interaction between the two leads to the penetration of the rock bridge, it belongs to the M-type rock bridge penetration mode.

From Fig. 13, it can be seen that the secondary cracks initiate and propagate in the rock bridge area, which makes the rock bridge cut through. After a certain distance of wing crack propagation, high shear stress concentration occurs in the rock bridge area, so that the shear action dominates between the cracks. However, previous studies have shown that tensile failure is the main failure mode of rock samples with double cracks under uniaxial compression [49]. It can be seen that the freeze-thaw cycle process may change the failure mode of the rock sample. Combined with Fig. 4 and Tables 3 and it can be seen that there are a lot of damage on the surface of rock samples after freeze-thaw cycle treatment, especially the rock samples with rock bridge dip angles of 60° (Fig. 4c), 75° (Fig. 4d) and 90° (Fig. 4e). In the process of freezing and thawing, there is a large amount of water in the cracks of rock samples. Under the action of freezing, water becomes ice and frost heave occurs. The frost heaving force acting on the tip of the prefabricated crack shows stress concentration [50]. In the repeated freeze-thaw cycles, the micro-cracks in the rock sample will gradually increase, and the frost heaving force will gradually increase. As a result, tensile cracks appear at the crack tip, which is particularly significant in Fig. 4c, d and e. Under the action of external load, the stress concentration effect at the crack tip is weakened. During the failure process, the number of tensile cracks generated at the crack tip gradually decreases, and the degree of development gradually decreases.

Under the action of external load, the crack will first extend along the frost heave crack and show the shape of the shear crack, as shown in Fig. 12a–c, and d. At the same time, it is found that when the two prefabricated cracks are collinear, the rock bridge area is more likely to have an S-shaped penetration mode (Fig. 8), Shen et al. [51] also mentioned a similar phenomenon in their related research papers. The T-type coalescence is only formed by the two wing cracks initiated at the tip II of the crack. M-type penetration, shear cracks first initiate and penetrate part of the rock bridge area, and then wing cracks appear to connect its tip, and finally penetrate the rock bridge area. Admittedly, the test results show a significant effect of shear stress. However, in fact, this is due to the effect of frost heaving force [52]. When the dip angle of rock bridge is 60° (M-type), the real-time evolution process of strain field and relative displacement curve is shown in Fig. 13. The relative displacement evolution characteristics of the feature points (a,b) on both sides of the fracture surface can quantitatively determine the fracture type: If the relative displacement shows a trend of separation and opening, it is a tensile crack; if there is a trend of shear dislocation, it is a shear fracture [53].

From Fig. 14, the horizontal longitudinal displacement of the characteristic points a and b along the y axis is positive on one side of the fracture surface and negative on the other side, indicating that the fracture is open. The trend shows that the fracture is open, and the opening degree gradually increases with the increase of loading time (Fig. 14b). The evolution curves of x-direction displacement on both

sides of the fracture are basically consistent, that is, under the action of compressive stress, the trend of synergistic decline is presented, and the shear dislocation is very small (Fig. 14a). According to the evolution characteristics of the relative displacement curves of the feature points a and b, it can be seen that the crack has not yet initiated before the protruding point A (184s), and the relative displacements in the x and y directions are basically the same. Subsequently, the cracks began to initiate and expand steadily. In this process, the relative displacement in the x di-rection remained basically unchanged, while the relative displacement in the y direction showed an open trend, which indicated that the expansion of the prefabricated cracks was dominated by tensile stress, and the rock had tensile failure. At 263 s, the relative displacement in the y direction in-creases rapidly, and the relative displacement in the x direction also increases slowly, which indi-cates that the crack begins to enter the unstable development stage. Until 278 s, the crack was un-stable and expanded, and at 300 s, the sample completely failed.

It can be seen that the freeze-thaw cycle will have a certain impact on the failure mode of rock bridge. Under the action of compressive stress, the crack will first extend along the frost heave crack. Although it ex-hibits the shape of a shear crack in appearance, the driving force of crack propagation is actually tensile stress.

4. Discussions

Through the analysis of the mechanical properties and failure modes of the samples with different dip angles of the rock bridge, it is found that with the increase of the dip angle of the rock bridge, the peak strength of the rock sample shows an inverted "spoon-shaped" trend of increasing first and then decreasing. The peak strength of rock bridge dip angle $\beta = 45°$ is the maximum, and it is also the turning point. The dynamic disturbance caused by open-pit mining in cold regions makes the mechanical properties of rock mass, the mechanism of catastrophic expansion of structural plane and the bearing capacity complicated. In order to ensure the safety of open-pit mine slope mining and improve economic benefits, it is necessary to discuss the above inverted "spoon-shaped" trend and turning point, so as to avoid the threat to safety and economic benefits caused by landslides caused by misestimating the bearing capacity of rock mass.

4.1. Numerical model establishment and analysis

Based on the effective and accurate discrete element method, the numerical models of different rock bridge dip angles are established. The effects of crack initiation and propagation on specimens with different rock bridge dip angles under compression are analyzed in detail. In order to compare, the loading rate (0.02 mm/min), sample size (50 mm * 100 mm) and crack size are used in the numerical simulation. The numerical model is established, as shown in Fig. 15.

Through the above laboratory tests, it can be seen that the peak strength increases when the rock bridge dip angle β is 30°–45°, and the peak strength decreases when the rock bridge dip angle β is 45°–60°.
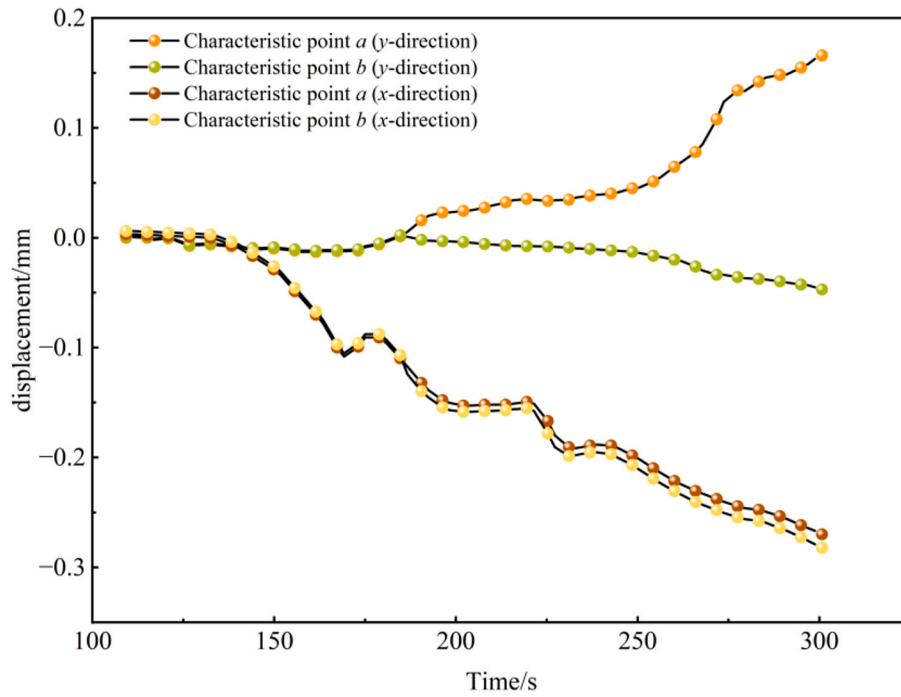
(a) The displacement evolution curves of feature points a, b in x, y directions.
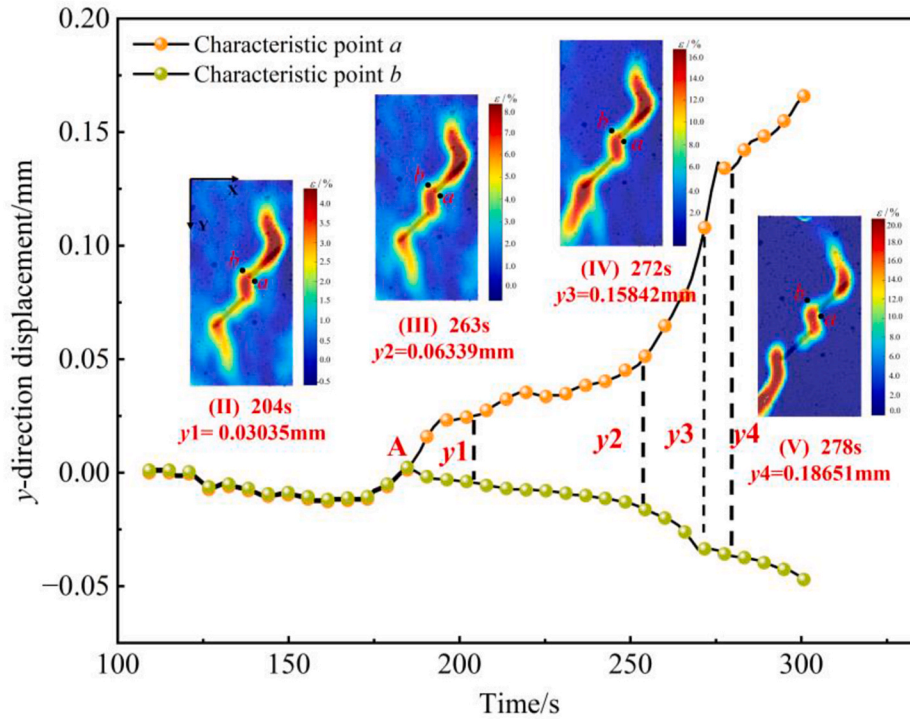
(b) y-direction crack opening

Fig. 14. Relative displacement evolution curve and strain field evolution characteristics of feature points on both sides of fracture surface.

When the rock bridge dip angle $\beta = 45°$, the peak strength is the largest. The rock bridge inclination angle β is set to 30°, 35°, 40°, 45°, 50°, 55° and 60° to verify whether the peak strength is still increasing first and then decreasing.

The freeze-thaw cycle simulation of rock samples with different rock bridge inclination angles is carried out. Under 80 freeze-thaw cycles, the stress field distribution of fractured rock samples with different rock bridge dip angles is shown in Fig. 16 (For example, $\beta = 45°$, 60°). The

stress-strain curves of specimens with different rock bridge inclination angles under uniaxial compression are shown in Fig. 16.

From Fig. 16, during the freeze-thaw cycle, stress concentration occurs at both the inner and outer tips of the crack. With the increase of the inclination angle of the rock bridge, the stress gradually increases and the stress concentration is more significant. This is because during the freezing process, water is converted into ice and frost heave occurs. The frost heaving force in the crack causes the stress concentration at the
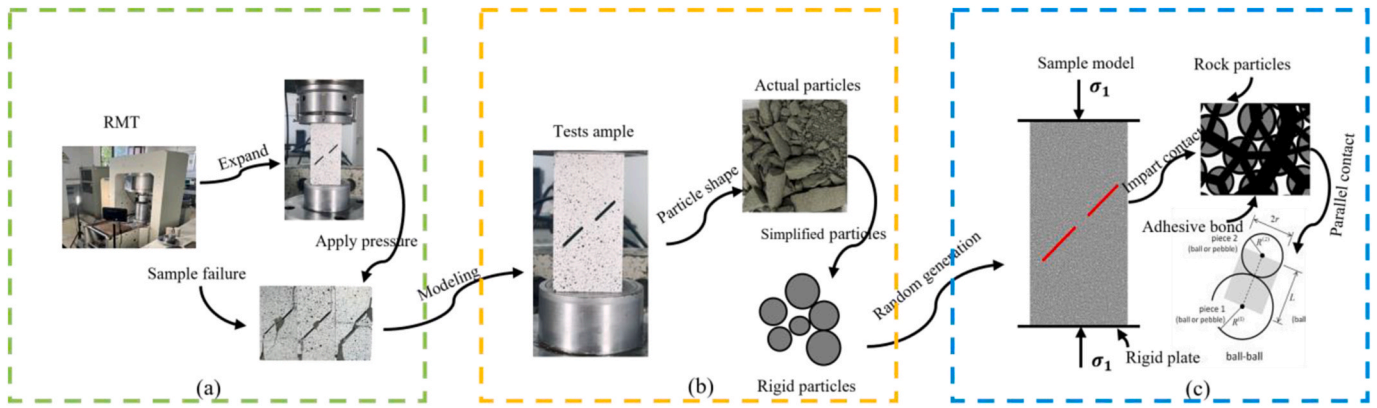
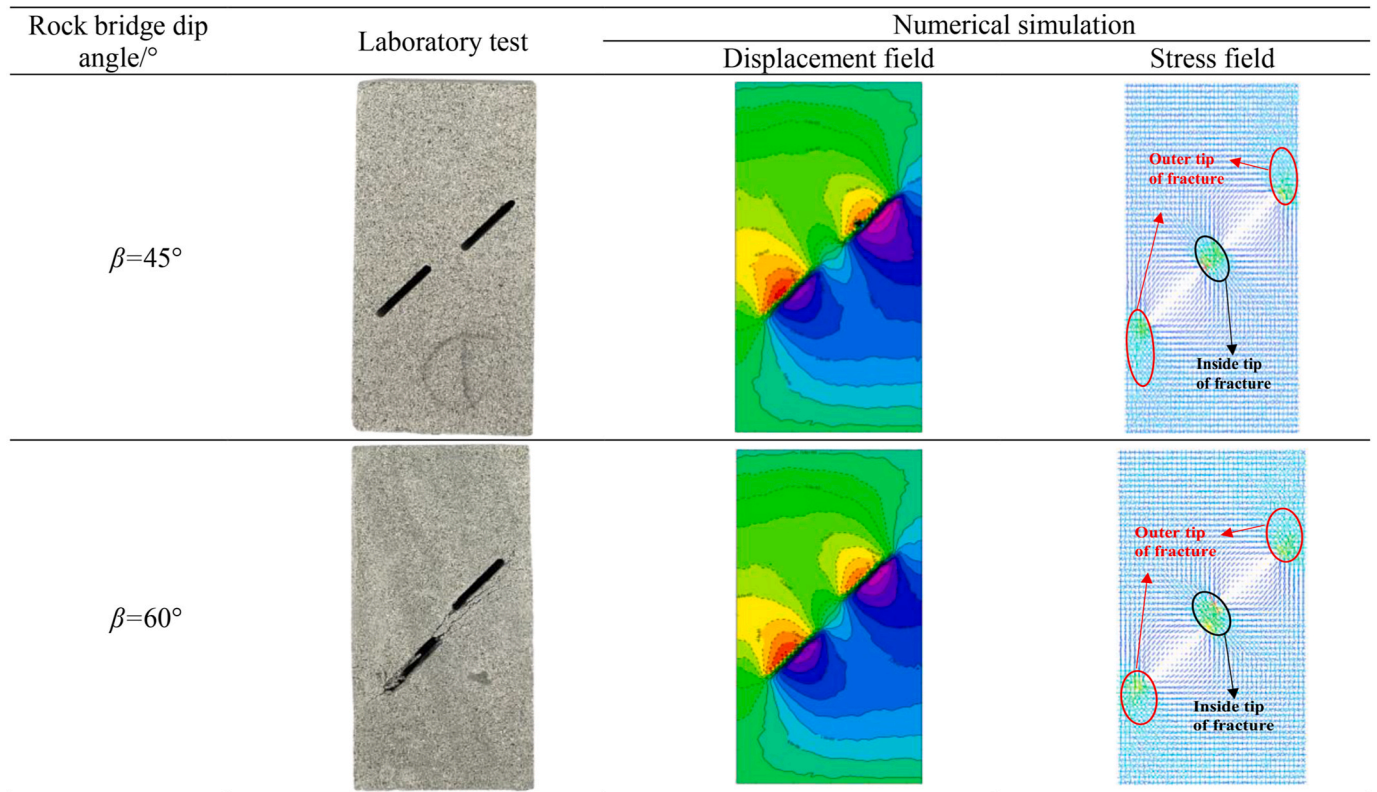**Fig. 15.** Numerical model establishment process.

Fig. 16. Multi-field distribution of fractured rock surface during freeze-thaw process.

crack tip, which makes the particles around the crack produce a certain tensile force on the crack, and then causes the local damage at the crack tip.

From Fig. 15, when the rock bridge dip angle β is 30°, 35°, 40°, 45°, the peak strength keeps rising. When the dip angle of rock bridge is 45°, 50°, 55 °and 60°, the compressive strength keeps decreasing. When the dip angle of rock bridge is 45°, the compressive strength is the largest.

In summary, we have conducted a more detailed study of the peak stress trend of the inverted spoon type shown in the test results, through numerical simulation, as shown in Fig. 17c. After the mutual demonstration of test and numerical simulation, the trend of peak stress still shows an inverted "spoon-shaped". For the cause of this inverted ' spoon ' trend, the research results of previous scholars provide some references, that is, the change of the dip angle of the rock bridge will affect the strength of the rock by affecting the failure mode of the fractured rock [54,55]. Therefore, it can be inferred that the rock bridge

penetration mode is the main reason for the ' inverted spoon ' of the peak stress trend. However, its mechanism of action needs further study.

5. Conclusion

In this paper, the fractured rock samples with different dip angles of rock bridge are taken as the research object, and the influence of different dip angles of rock bridge on rock mechanical properties, crack propagation and fracture mechanism is analyzed The mechanism of three failure modes of rock bridge penetration is revealed, and the causes of the inverted ' spoon-shaped ' rock strength trend are discussed. The following conclusions are obtained.

(1) Under the action of freeze-thaw cycle, the internal pores and cracks of rock samples gradually develop, which makes the stress-strain curve appear obvious nonlinear compaction section. The
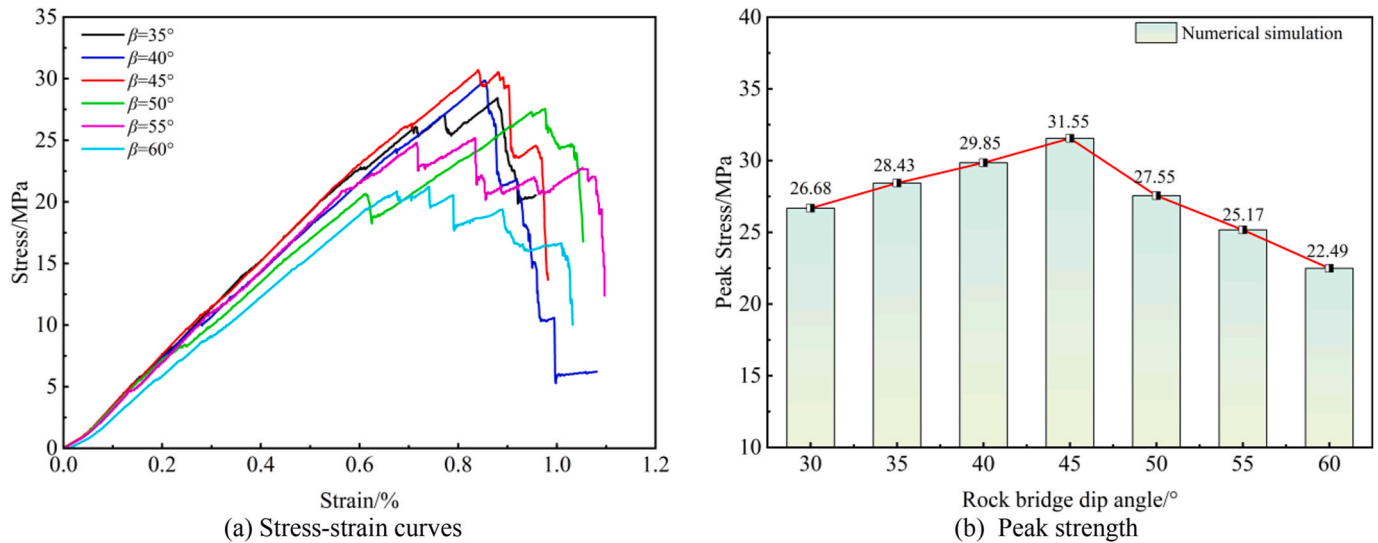
Fig. 17. Stress-strain curves and peak strength of different dip angles of rock bridge.

development and propagation of cracks will lead to a significant stress drop in the stress-strain curve. When the crack propagates and penetrates, the curve will drop to a certain extent. When the rock bridge area is damaged and penetrated, the sample is unstable.

(2) The frost heaving force caused by freezing and thawing will cause irreversible damage to rock samples. Especially at the tip of the prefabricated crack, macroscopic frost heave cracks will occur. Frost heaving cracks can reduce the stress concentration at the crack tip, which leads to a decrease in tensile cracks during loading.

(3) With the increase of the dip angle β of the rock bridge, the three kinds of modulus (initial modulus, secant modulus, elastic modulus) and the peak value show an inverted "spoon-shaped" evolution law, which increases first and then decreases. When $\beta = 45°$, the values and peak strength of the three modulus are the largest. When the dip angle of rock bridge is the same, the size of the three kinds of modulus is shown as elastic modulus > secant modulus > initial modulus.

(4) The freeze-thaw cycle has a significant effect on the failure mode of the sample. The tensile effect of the frost heave force generated by the freeze-thaw process leads to the early development and expansion of the prefabricated cracks. Under the action of external load, according to the law of crack development, the failure mode of rock bridge can be divided into shear failure (S type), tensile failure (T type) and tensile-shear composite failure (M type).

(5) In the initial deformation stage of rock, the relative displacement evolution curves of feature points on both sides of the fracture are consistent. With the continuous deformation, the relative displacement evolution curves of feature points deviate from each other. The y-direction displacement curve deviates, the crack propagation is dominated by tensile stress, the x-direction displacement curve deviates, and the crack propagation is dominated by shear stress. For tensile-shear composite failure (M-type), the occurrence of shear cracks is due to the action of frost heaving force, so it shows a shear failure mode, and the internal force is tension.

(6) The peak stress of rock shows inverted "spoon-shaped", and its formation mechanism is quite complex, which is affected by the interaction of many factors. In the future research, it is necessary to construct a multi-factor coupling model, which needs to consider the non-uniformity of the internal fracture distribution of the rock bridge, the mode of action of the external load and the freeze-thaw cycle. Through this model, the transfer law of freeze-thaw erosion in the stress concentration area inside the rock during the process of rock bridge penetration, and the initiation and propagation of cracks under the combined action of freeze-thaw and external force are explored. At the same time, the stress singularity at the crack tip and the interaction force between the cracks should be analyzed in detail when the rock bridge is connected, especially how the freeze-thaw cycle participates in and affects these processes, and the problems related to engineering safety may be caused.

CRediT authorship contribution statement

Meilu Yu: Writing – review & editing, Writing – original draft, Supervision, Software, Resources, Funding acquisition. **Zhongwen Wang:** Writing – original draft, Funding acquisition, Formal analysis, Data curation. **Ying Xu:** Supervision, Resources, Funding acquisition. **Yanhai Chang:** Supervision, Data curation. **Luyu Wang:** Software. **Yulong Zhu:** Methodology, Investigation.

Data availability

Data will be made available on request.

Funding statement

Declaration of competing interest

We would like to submit the enclosed manuscript entitled The failure behavior of prefabricated fractured sandstone with different rock bridge inclination angles under freeze-thaw cycles, which we wish to be considered for publication in Unconventional Resources. The work described has not been submitted elsewhere for publication, in whole or in part, and all the authors listed have approved the manuscript that is

enclosed. There are no conflicts of interest to declare.

Comments from you and the reviewers will be highly appreciated. Thank you very much for your time and consideration.

References

[1] Y. Wu, X. Li, L. Zhu, Fracture mechanism of rock collapse in the freeze–thaw zone of the eastern Sichuan–Tibet Mountains under seasonal fluctuating combinations of water and heat, Nat. Hazards 108 (2) (2021) 2309–2333, https://doi.org/10.1007/s11069-021-04781-y.

[2] C. Guo, Y. Zhang, Y. Zhang, et al., Freeze-thaw cycle effects on granite and the formation mechanism of long-runout landslides: insights from the Luanshibao case study in the Tibetan Plateau, China, Bull. Eng. Geol. Environ. 82 (10) (2023) 394, https://doi.org/10.1007/s10064-023-03427-6.

[3] S. Sardana, R.K. Sinha, A.K. Verma, M. Jaswal, T.N. Singh, Influence of freeze–thaw on the stability of road cut slopes—a case study in the Indian Himalayan region, CaGeJ 60 (1) (2022) 107–112, https://doi.org/10.1139/cgj-2021-0378.

[4] Q. Yu, P. Lei, Z. Dai, Damage characteristics of limestone under freeze–thaw cycle for tunnels in seasonal frozen areas, Iran, J. Sci. Technol. Trans. A. Sci. 47 (1) (2023) 469–477, https://doi.org/10.1007/s40996-022-00979-7.

[5] A. Bobet, H.H. Einstein, Fracture coalescence in rock-type materials under uniaxial and biaxial compression, Int. J. Rock Mech. Min. Sci. 35 (7) (1998) 863–888, https://doi.org/10.1016/S0148-9062(98)00005-9.

[6] G. Tan, C. Ma, J. Zhang, W. Yang, G. Zhang, Z. Kang, Mechanical behavior of rock under uniaxial tension: insights from energy storage and dissipation, J. Rock Mech. Geotech. Eng. 16 (7) (2024) 2466–2481, https://doi.org/10.1016/j.jrmge.2023.12.022.

[7] J. Yahaghi, H. Liu, A. Chan, D. Fukuda, Experimental and numerical studies on failure behaviours of sandstones subject to freeze-thaw cycles, Transport Geotech 31 (2021) 100655, https://doi.org/10.1016/j.trgeo.2021.100655.

[8] Y. Zhou, Z. Zhou, Y. Shen, et al., Interaction of two offset parallel flaws in geomaterials under unloading conditions, Theor. Appl. Fract. Mech. 125 (2023) 103894, https://doi.org/10.1016/j.tafmec.2023.103894.

[9] G. Chen, Y. Wan, Y. Li, X. Pei, D. Huang, Time-dependent damage mechanism of rock deterioration under freeze–thaw cycles linked to alpine hazards, Nat. Hazards 108 (1) (2021) 635–660, https://doi.org/10.1007/s11069-021-04699-5.

[10] M. Deprez, T. De Kock, G. De Schutter, V. Cnudde, A review on freeze-thaw action and weathering of rocks, Earth Sci. Rev. 203 (2020) 103143, https://doi.org/10.1016/j.earscirev.2020.103143.

[11] G. Cheng, T. Wei, J. Ma, Z. Wu, Study on the stepped failure of rock slopes and fracture mechanism of rock bridges Chinese, Journal of Rock Mechanics and Engineering 43 (4) (2024) 809–821, https://doi.org/10.13722/j.cnki.jrme.2023.0603.

[12] D. Fakhri, A. Mahmoodzadeh, A. Hussein Mohammed, et al., Forecasting failure load of Sandstone under different Freezing-Thawing cycles using Gaussian process regression method and grey wolf optimization algorithm, Theor. Appl. Fract. Mech. 125 (2023) 103876, https://doi.org/10.1016/j.tafmec.2023.103876.

[13] A. Mu, Y. Du, H. Zhang, M. Xie, N. Jiang, S. Li, J. Liu, Review on the monitoring and early warning technology of large-scale unstable rock collapse, Advanced Engineering Sciences 56 (5) (2024) 10–23. https://link.cnki.net/urlid/51.1773.tb.20240619.1427.002.

[14] Y. Song, C. Li, R. BI, K. Zhang, Y. Zhou, D. Han, Study on characteristics of pore propagation and evolution in freeze-thawed rock, J. Glaciol. Geocryol. 45 (3) (2023) 1116–1127. https://link.cnki.net/10.7522/j.issn.1000-0240.2023.0086.

[15] X. Wang, H. Xie, R. Zhang, et al., Progressive failure characterization of sandstone from yingjinshan area in Qinghai-Tibet Plateau, Rock Mech. Rock Eng. 55 (11) (2022) 6723–6740, https://doi.org/10.1007/s00603-022-02999-1.

[16] X. Zhou, Y. Fu, Y. Wang, J. Zhou, Experimental study on the fracture and fatigue behaviors of flawed sandstone under coupled freeze–thaw and cyclic loads, Theor. Appl. Fract. Mech. 119 (2022) 103299, https://doi.org/10.1016/j.tafmec.2022.103299.

[17] M. Asadizadeh, S. Khosravi, J. Karimi, T. Sherizadeh, S. Vajedian, M.F. Hossaini, Mechanical behavior of single-flawed cylindrical specimens subjected to axial loading: a numerical investigation, Bull. Eng. Geol. Environ. 81 (10) (2022) 442, https://doi.org/10.1007/s10064-022-02940-4.

[18] S. Patel, C.D. Martin, Impact of the initial crack volume on the intact behavior of a bonded particle model, Comput. Geotech. 127 (2020) 103764, https://doi.org/10.1016/j.compgeo.2020.103764.

[19] P.L.P. Wasantha, D. Bing, S. Yang, M. Xu, Numerical modelling of the crack-pore interaction and damage evolution behaviour of rocklike materials with pre-existing cracks and pores, IJDM 30 (2020) 720–738.

[20] L. Weng, Z. Wu, A. Taheri, Q. Liu, H. Lu, Deterioration of dynamic mechanical properties of granite due to freeze-thaw weathering: considering the effects of moisture conditions, Cold Reg. Sci. Technol. 176 (2020) 103092, https://doi.org/10.1016/j.coldregions.2020.103092.

[21] P. Shan, W. Li, X. Lai, S. Zhang, X. Chen, X. Wu, Research on the response mechanism of coal rock mass under stress and pressure, Mater 16 (8) (2023) 3235. https://www.mdpi.com/1996-1944/16/8/3235.

[22] S. Yang, J. Dong, J. Yang, Z. Yang, Y. Huang, An experimental investigation of failure mechanical behavior in cylindrical granite specimens containing two non-coplanar open fissures under different confining pressures, J. Cent. South Univ. 29 (5) (2022) 1578–1596, https://doi.org/10.1007/s11771-022-5035-4.

[23] T. Han, Z. Li, Mechanical characteristics and failure modes for mode-I sandstone and rock-like cracked sample exposed to freeze thawing cycle, Bull. Eng. Geol. Environ. 80 (9) (2021) 6937–6953, https://doi.org/10.1007/s10064-021-02347-7.

[24] J.-X. Ren, M.-C. Yun, X.-T. Cao, K. Zhang, Y. Liang, X. Chen, Study on the mechanical properties of saturated red sandstone under freeze–thaw conditions, Environ. Earth Sci. 81 (14) (2022) 376, https://doi.org/10.1007/s12665-022-10503-9.

[25] S. Yu, Y. Ke, H. Deng, G. Tian, J. Deng, Experimental investigation of porous and mechanical characteristics of single-crack rock-like material under freeze-thaw weathering 11 (12) (2021) 1318.

[26] M. Asadizadeh, M.F. Hossaini, M. Moosavi, H. Masoumi, P.G. Ranjith, Mechanical characterisation of jointed rock-like material with non-persistent rough joints subjected to uniaxial compression, Eng. Geol. 260 (2019) 105224, https://doi.org/10.1016/j.enggeo.2019.105224.

[27] J. Hu, H. Pan, L. Li, et al., Experimental and numerical study of joint persistence effect on the non-persistent jointed rock mass' tension failure behavior, Rock Mech. Rock Eng. 56 (12) (2023) 9121–9134, https://doi.org/10.1007/s00603-023-03538-2.

[28] M. Naderloo, M. Moosavi, M. Ahmadi, Using acoustic emission technique to monitor damage progress around joints in brittle materials, Theor. Appl. Fract. Mech. 104 (2019) 102368, https://doi.org/10.1016/j.tafmec.2019.102368.

[29] V. Sarfarazi, H. Haeri, Effect of number and configuration of bridges on shear properties of sliding surface, J. Min. Sci. 52 (2) (2016) 245–257, https://doi.org/10.1134/S1062739116020370.

[30] Z. Aliabadian, M. Sharafisafa, F. Tahmasebinia, L. Shen, Experimental and numerical investigations on crack development in 3D printed rock-like specimens with pre-existing flaws, Eng. Fract. Mech. 241 (2021) 107396, https://doi.org/10.1016/j.engfracmech.2020.107396.

[31] Q. Lin, P. Cao, G. Wen, J. Meng, R. Cao, Z. Zhao, Crack coalescence in rock-like specimens with two dissimilar layers and pre-existing double parallel joints under uniaxial compression, Int. J. Rock Mech. Min. Sci. 139 (2021) 104621, https://doi.org/10.1016/j.ijrmms.2021.104621.

[32] J. Qi, L. Zhou, H. Zhang, J. Chen, L. Ma, T. Shi, Research on crack evolution law and mechanical analysis of three cracked rock masses subjected to compression load, Theor. Appl. Fract. Mech. 127 (2023) 104035, https://doi.org/10.1016/j.tafmec.2023.104035.

[33] Y.-H. Huang, S.-Q. Yang, W.-L. Tian, Crack coalescence behavior of sandstone specimen containing two pre-existing flaws under different confining pressures, Theor. Appl. Fract. Mech. 99 (2019) 118–130, https://doi.org/10.1016/j.tafmec.2018.11.013.

[34] J. Lee, J.-W. Hong, J.-W. Jung, The mechanism of fracture coalescence in pre-cracked rock-type material with three flaws, Eng. Geol. 223 (2017) 31–47, https://doi.org/10.1016/j.enggeo.2017.04.014.

[35] D.-J. Wang, H. Tang, D. Elsworth, C. Wang, Fracture evolution in artificial bedded rocks containing a structural flaw under uniaxial compression, Eng. Geol. 250 (2019) 130–141, https://doi.org/10.1016/j.enggeo.2019.01.011.

[36] M. Sharafisafa, L. Shen, Q. Xu, Characterisation of mechanical behaviour of 3D printed rock-like material with digital image correlation, Int. J. Rock Mech. Min. Sci. 112 (2018) 122–138, https://doi.org/10.1016/j.ijrmms.2018.10.012.

[37] X.P. Zhou, Y.J. Lian, L.N.Y. Wong, F. Berto, Understanding the fracture behavior of brittle and ductile multi-flawed rocks by uniaxial loading by digital image correlation, Eng. Fract. Mech. 199 (2018) 438–460, https://doi.org/10.1016/j.engfracmech.2018.06.007.

[38] D. Shirole, G. Walton, A. Hedayat, Experimental investigation of multi-scale strain-field heterogeneity in rocks, Int. J. Rock Mech. Min. Sci. 127 (2020) 104212, https://doi.org/10.1016/j.ijrmms.2020.104212.

[39] M. Ju, H. Xing, Crack propagation in jointed rock and its effect on rock macrofracture resistance: insights from discrete element analysis, Geomech. Geophys. Geo-energ. Geo-resour. 8 (2022) 21, https://doi.org/10.1007/s40948-021-00326-6.

[40] S. Zare, S. Karimi-Nasab, H. Jalalifar, Analysis and determination of the behavioral mechanism of rock bridges using experimental and numerical modeling of non-persistent rock joints, Int. J. Rock Mech. Min. Sci. 141 (2021) 104714, https://doi.org/10.1016/j.ijrmms.2021.104714.

[41] G. Xu, M. Gutierrez, Z. Hou, X. Li, Propagation and coalescence of two infilled parallel fractures in shale: laboratory testing and DEM simulations, Granul. Matter 24 (2) (2022) 53, https://doi.org/10.1007/s10035-022-01207-9.

[42] S.-Y. Wu, Y.-H. Huang, Macro and meso crack evolution of granite specimens with non-straight fissures: a comparison between two bond models, Theor. Appl. Fract. Mech. 125 (2023) 103890.

[43] N. Liu, Y. Yang, N. Li, S. Liang, H. Liu, C. Li, The stability issue of fractured rock mass slope under the influences of freeze–thaw cycle, Sci. Rep. 14 (1) (2024) 5674, https://doi.org/10.1038/s41598-024-56346-1.

[44] Y. Sheng, G. Yang, T. Rong, H. Liu, L. Wuyang, Proposed scheme for freeze-thaw cycle tests on rock, Chin. J. Geotech. Eng. 38 (10) (2016) 1775–1782. https://link.cnki.net/10.11779/CJGE201610005.

[45] Q. Zhang, Y. Liu, F. Dai, A frost heave pressure model for fractured rocks subjected to repeated freeze-thaw deterioration, Eng. Geol. 337 (2024) 107587, https://doi.org/10.1016/j.enggeo.2024.107587.

[46] N. Peng, J. Hong, Y. Zhu, Y. Dong, B. Sun, J. Huang, Experimental investigation of the influence of freeze–thaw mode on damage characteristics of sandstone, Appl. Sci. Basel. 12 (23) (2022) 12395, https://doi.org/10.3390/app122312395.

[47] T. Zhu, J. Chen, D. Huang, A DEM-based approach for modeling the damage of rock under freeze–thaw cycles, Rock Mech. Rock Eng. 54 (2021) 2843–2858, https://doi.org/10.1007/s00603-021-02465-4.

[48] A. Bobet, The initiation of secondary cracks in compression, Eng. Fract. Mech. 66 (2) (2000) 187–219, https://doi.org/10.1016/S0013-7944(00)00009-6.

[49] S.R. Wang L, C.Q. Zhu, Study on the influences of rock bridge dip angle and mineral structure on coal, Chin. J. Rock Mech. Eng. 43 (9) (2024) 2108–2124, https://doi.org/10.13722/j.cnki.jrme.2023.1065.

[50] Y. Xu, Z. Wang, M. Yu, et al., Simulation study of the rupture mechanism of through-cracking under freeze–thaw load coupling effect, Nat. Hazards 120 (11) (2024) 9809–9831, https://doi.org/10.1007/s11069-024-06587-0.

[51] S.O. Shen B, H.H. Einstein, Ghahreman BJJoGR, Coalescence of fractures under shear stresses in experiments, J. Geophys. Res. Solid Earth 100 (1995) 5975–5990, https://doi.org/10.1029/95JB00040.

[52] T.X.-H. Li P, Q.S. Liu, P.D. Luo, Study on frost heave fracture characteristics and strength loss of double fissure sandstone, Chin. J. Rock Mech. Eng. 39 (1) (2020) 115–125, https://doi.org/10.13722/j.cnki.jrme.2019.0679.

[53] S.W. Wang Z, X. Wang, Surface deformation field and fracture propagation mechanism of rock-like specimen with pre-existing fracture, Coal Sci. Technol. 51 (10) (2023) 2108–2124, https://doi.org/10.13722/j.cnki.jrme.2023.1065.

[54] Z.D. Yang DF, S.J. Niu, Experimental study on crack propagation process and macroscopic failure mode of prefabricated-crack fine sandstone under uniaxial compression, Journal of Mining & Safety Engineering 36 (4) (2019) 786–793, https://doi.org/10.13545/j.cnki.jmse.2019.04.018.

[55] D.C. Zhu KR, R.D. Lei, Influence of grout-filled flaws on strength properties and fracture modes of coal petrography, Saf. Coal Mine 52 (2) (2021) 63–70, https://doi.org/10.13347/j.cnki.mkaq.2021.02.013.